Influence of lateral slab edge distance on plate velocity, trench velocity, and subduction partitioning

Article *in* Journal of Geophysical Research Atmospheres · October 2011

DOI: 10.1029/2011JB008535

CITATIONS
53

READS
3,426

4 authors:

Wouter P. Schellart
Vrije Universiteit Amsterdam (Netherlands)
138 PUBLICATIONS **4,738** CITATIONS
SEE PROFILE

Dave R Stegman
University of California, San Diego
59 PUBLICATIONS **2,468** CITATIONS
SEE PROFILE

Rebecca Farrington
University of Melbourne
16 PUBLICATIONS **387** CITATIONS
SEE PROFILE

Louis Moresi
Australian National University
324 PUBLICATIONS **9,241** CITATIONS
SEE PROFILE

Influence of lateral slab edge distance on plate velocity, trench velocity, and subduction partitioning

W. P. Schellart,[1] D. R. Stegman,[2] R. J. Farrington,[3] and L. Moresi[1,3]

Received 18 May 2011; revised 8 August 2011; accepted 8 August 2011; published 27 October 2011.

[1] Subduction of oceanic lithosphere occurs through both trenchward subducting plate motion and trench retreat. We investigate how subducting plate velocity, trench velocity and the partitioning of these two velocity components vary for individual subduction zone segments as a function of proximity to the closest lateral slab edge (D_{SE}). We present a global compilation for 207 trench segments from 17 active subduction zones on Earth and three-dimensional numerical models of progressive free subduction of a single oceanic plate that subducts into a stratified mantle. The results show that the subducting plate velocity is always high (≥5.1 cm/yr (models) and ≥4.2 cm/yr (nature)) and trench velocity is always low (≤2.5 cm/yr (models) and ≤1.7 cm/yr (nature)) in the center of wide subduction zones (D_{SE} > 2200 km). Only in regions close to lateral slab edges (D_{SE} < 1000 km), be it for narrow or wide subduction zones, can the trench velocity exceed 4 cm/yr (models) and 6 cm/yr (nature) and can the subducting plate velocity go below 4 cm/yr (models) and 2 cm/yr (nature). In general, plate velocities, trench velocities and subduction partitioning are much more variable near slab edges than in the center of wide subduction zones owing to other parameters that affect subduction kinematics. We conclude that subduction kinematics can vary considerably along individual subduction zones and that the upper bound values for trench velocity and lower bound values for subducting plate velocity and subduction partitioning at individual subduction zone segments depend critically on D_{SE}.

Citation: Schellart, W. P., D. R. Stegman, R. J. Farrington, and L. Moresi (2011), Influence of lateral slab edge distance on plate velocity, trench velocity, and subduction partitioning, *J. Geophys. Res.*, *116*, B10408, doi:10.1029/2011JB008535.

1. Introduction

[2] The Earth's oceanic lithosphere disappears into the mantle at subduction zones. The rate at which such lithosphere disappears, the subduction velocity ($v_{S\perp}$), depends on the trench-normal subducting plate velocity ($v_{SP\perp}$) and the trench-normal trench velocity ($v_{T\perp}$). Indeed, the subduction velocity is simply the sum of $v_{SP\perp}$ and $v_{T\perp}$. What determines the magnitude of $v_{SP\perp}$ and $v_{T\perp}$, and how subduction is partitioned between its two components has been an active field of research in the last two decades [e.g., *Zhong and Gurnis*, 1995; *Schellart*, 2004, 2008a; *Stegman et al.*, 2006, 2010a; *Faccenna et al.*, 2007; *Di Giuseppe et al.*, 2008]. Subduction partitioning provides a strong control on slab geometry [*Di Giuseppe et al.*, 2008; *Schellart*, 2008a; *Stegman et al.*, 2010a] and the style of mantle stirring [*Buttles and Olson*, 1998; *Kincaid and Griffiths*, 2004; *Schellart*, 2004, 2008a; *Funiciello et al.*, 2004; *Stegman et al.*, 2006], i.e., poloidal versus toroidal flow, thereby providing constraints on the geochemical heterogeneity of the mantle [*Stegman et al.*, 2002; *van Keken et al.*, 2002]. Furthermore, understanding of subduction partitioning ($v_{SP\perp}/v_{S\perp}$) is vital for constraining its effect on shear wave splitting and mantle anisotropy [*Russo and Silver*, 1994; *Buttles and Olson*, 1998; *Long and Silver*, 2008].

[3] Previous research suggests that plate velocity is controlled by the plate boundary fraction that is a subduction margin [*Forsyth and Uyeda*, 1975; *Gripp and Gordon*, 1990], but this cannot explain the variation of $v_{T\perp}$ and $v_{SP\perp}/v_{S\perp}$. Other research suggests that an increase in plate age corresponds to an increase in subducting plate velocity [*Carlson et al.*, 1983; *Goes et al.*, 2008] and trench retreat velocity [*Molnar and Atwater*, 1978], but initial work from *Jarrard* [1986] and more recent work from *Heuret and Lallemand* [2005] implies no correlation exists between plate age and trench velocity. Most recently, a global compilation of subduction zones has shown that the correlation between subducting plate age and both $v_{SP\perp}$ and $v_{T\perp}$ is relatively weak [*Schellart et al.*, 2010]. It thus appears that the aforementioned individual parameters cannot explain the diversity of subduction partitioning, plate velocities and trench velocities on Earth.

[4] A new hypothesis to explain the variation of $v_{SP\perp}$, $v_{T\perp}$ and $v_{SP\perp}/v_{S\perp}$ for active subduction zones on Earth has been

[1]School of Geosciences, Monash University, Melbourne, Victoria, Australia.
[2]Scripps Institution of Oceanography, University of California, San Diego, La Jolla, California, USA.
[3]School of Mathematical Sciences, Monash University, Melbourne, Victoria, Australia.

0148-0227/11/2011JB008535

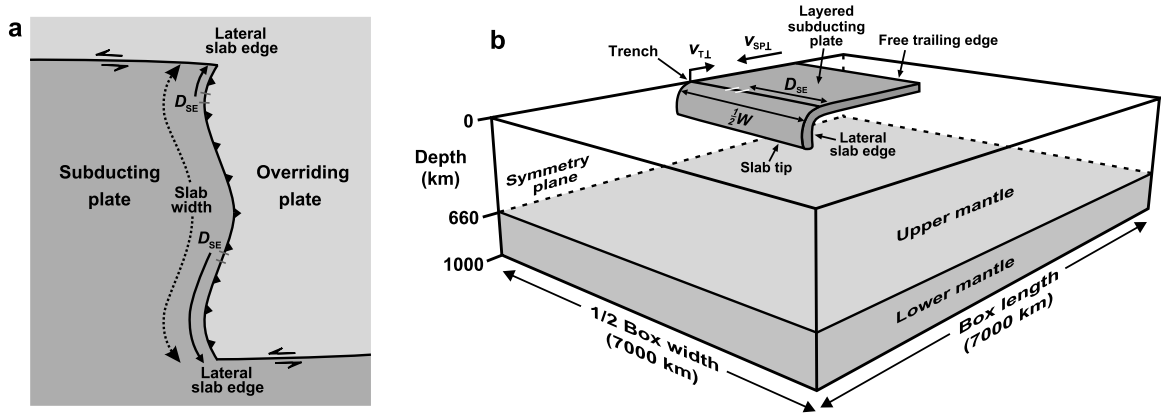

Figure 1. (a) Schematic map view illustration of a subduction zone showing the parameters W (subduction zone slab width) and D_{SE} (the distance of the center of a trench segment to its closest lateral slab edge). (b) Numerical model set-up with a dense high-viscosity plate (representing mature oceanic lithosphere) overlying a lower-density layered linear viscous mantle confined in a three-dimensional Cartesian box. The upper mantle is 660 km thick with a low viscosity upper mantle (η_{UM}) and is underlain by 340 km of higher viscosity lower mantle (100 η_{UM}). The plate is 100 km thick and consists of four 25-km-thick layers, with a viscoplastic top layer (von Mises yield function with maximum viscosity of 1000 η_{UM}) followed by three linear-viscous layers for which the viscosity decreases from top to bottom (300 η_{UM}, 50 η_{UM} and 10 η_{UM}). Boundary conditions on the sidewalls, the top surface and the bottom surface are free-slip. Subduction is driven entirely by buoyancy forces, reflecting natural subduction systems. W indicates slab width, which is varied for each simulation and ranges between 300 km and 7000 km. D_{SE} indicates the distance between the center of a trench segment (200 km in trench-parallel extent for models and nature) and the closest lateral slab edge. Each experiment starts with a 187 km long slab perturbation dipping at 15.5°. Note that only half of the model domain is shown (and calculated), because the experiments are geometrically symmetrical with respect to a plane through the center of the subduction zone (symmetry plane) and because flow in the experiments occurs at low Reynolds number (Re $\ll$ 1) and is thus in a laminar symmetrical flow regime.

presented recently and is based on a global data set of subduction zone kinematics, 3D numerical models of progressive free subduction and a new scaling formulation [*Schellart et al.*, 2010]. In this new hypothesis, the variation in $v_{SP\perp}$, $v_{T\perp}$ and $v_{SP\perp}/v_{S\perp}$ at subduction zones is explained with the trench-parallel extent of their slabs, i.e., their width (W, Figure 1a), where $v_{SP\perp}$ scales with $\sim W^{2/3}$ and $v_{T\perp}$ scales with $\sim W^{-1}$. The lateral extent of subducted slabs is determined by the distance between its lateral slab edges. Such lateral slab edges might form at subduction zone-transform fault plate boundary corners [e.g., *Millen and Hamburger*, 1998; *Govers and Wortel*, 2005; *Wortel et al.*, 2009], due to slab segmentation along subvertical slab tears [e.g., *Rosenbaum et al.*, 2008; *Wortel et al.*, 2009; *Yang et al.*, 2009], or due to subduction of spreading ridges [e.g., *Dickinson and Snyder*, 1979; *Thorkelson*, 1996; *Thorkelson et al.*, 2011].

[5] The parameter D_{SE}, the distance of a subduction zone trench segment to its closest lateral slab edge (Figure 1a), is closely related to slab width and might provide insights into the potential variation in kinematics and dynamics along individual subduction zones (i.e., along the trench). Previous works have demonstrated a dependence of $v_{T\perp}$ on D_{SE}, but only using data from subduction zones in nature [*Schellart et al.*, 2007, 2008]. In this contribution, we will expand on these works by illustrating the dependence of $v_{T\perp}$, $v_{SP\perp}$ and $v_{SP\perp}/v_{S\perp}$ on D_{SE}. We will do this by presenting results from a global data set of active subduction zones on Earth (using four different global reference frames), and also by using geodynamic 3D numerical models of progressive free subduction. The geodynamic models provide a physical basis for the influence exerted by lateral slab edges on the variation in subduction zone kinematics along individual subduction zones.

2. Methods

2.1. Numerical Models

[6] The numerical simulations were done using the code *Underworld* [*Moresi et al.*, 2003; *Stegman et al.*, 2006, 2010a], in which subduction and plate motion are modeled in a three-dimensional Cartesian box by chemical convection in an incompressible Boussinesq fluid at infinite Prandtl number and very low Reynolds number. In *Underworld*, distinct volumes such as the subducting plate, upper mantle and lower mantle are represented by Lagrangian particles that are embedded within a standard Eulerian finite element mesh, which discretizes the problem and solves the governing equations. The nondimensional equations describing the flow in the models and details on the numerical technique are described in detail elsewhere [*Moresi et al.*, 2003; *Stegman et al.*, 2006]. The numerical model design is based on earlier work [*Schellart et al.*, 2010]. Progressive subduction and plate motion were modeled in three-dimensional space using a dense four-layer oceanic plate (viscoplastic top and three viscous layers) overlying a less-dense stratified linear-viscous mantle (Figure 1b). The plate has a viscoplastic top layer (25 km thick, maximum viscosity of 1000 times that of the upper mantle, η_{UM}, represented by a

von Mises yield function) followed by three linear-viscous layers with a progressively decreasing viscosity (300 η_{UM}, 50 η_{UM} and 10 η_{UM}, each 25 km thick). The average viscosity of the slab is thus ~10^2 × η_{UM}, closely reflecting average viscosity ratios between slab and upper mantle as estimated previously for the natural prototype (~50–500 × η_{UM}) [*Wu et al.*, 2008; *Schellart*, 2008a; *Loiselet et al.*, 2009; *Capitanio et al.*, 2009; *Ribe*, 2010; *Stegman et al.*, 2010a]. The upper/lower mantle transition is represented as a viscosity discontinuity at a depth of 660 km with the lower mantle viscosity η_{LM} = 100 η_{UM}. We choose a linear viscous rheology for the entire sublithospheric mantle. The subducting plate is laterally homogeneous and has a total thickness representing 100 km in nature, corresponding to mature oceanic lithosphere (≥80 Ma) with a density contrast of 80 kg/m^3 with respect to the underlying mantle [*Cloos*, 1993].

[7] The plate has a free trailing edge representing a Pacific style subducting plate with a spreading ridge at its trailing edge that offers minimal resistance to plate motion. Due to geometrical symmetry with respect to the mid-plane of the subduction zone and due to the low Reynolds number, all experiments were run in a Cartesian box with only half the dimension in the trench-parallel direction (Figure 1b). Plates have an initial length of 2200 km of flat-lying lithosphere with an additional slab length of 187 km dipping at 15.5° to initiate progressive subduction. Slab width (W), i.e., its trench-parallel extent, varies for successive experiments between 300 and 7000 km, while box size is constant (7000 km long, 14000 km wide and 1000 km deep). Mesh resolution in all models is 140 (length) by 280 (width) by 40 (depth) with an initial particle distribution of 20 particles per cell. In all experiments, separation between lateral slab edge and lateral sidewall is always ≥0.5W, separation between the trench and front wall is always ≥0.5W and velocity boundary conditions are free-slip everywhere to minimize influence of the box sidewalls following *Schellart et al.* [2010]. In all simulations the box is large enough such that no appreciable amount of deformation occurs on the sidewalls, which verifies that the sidewall boundary conditions are not influencing the subduction dynamics or the induced flow significantly.

[8] The velocities in the models (v') were scaled to velocities on Earth (v) following

$$v = v'(\eta'_{UM}\Delta\rho g T_{SP} T_{UM})/(\eta_{UM}\Delta\rho' g' T'_{SP} T'_{UM}) \quad (1)$$

where $\Delta\rho$ is the density contrast between the subducting plate and upper mantle (80 kg/m^3), g is the gravitational acceleration (9.8 m/s^2), T_{SP} is the subducting plate thickness (100 km), T_{UM} is the upper mantle thickness (660 km) and η_{UM} is the upper mantle dynamic viscosity (1.57 × 10^{20} Pa s).

[9] We do not take into account the effects of thermal diffusion nor the presence of an overriding plate. Thus, the single plate subducts in isolation and is not affected by neighboring slabs or large-scale mantle flow. Due to the absence of an overriding plate, the subduction fault has the same viscosity as the ambient upper mantle and is thus very weak. Such low subduction fault strength is indeed implied by global considerations [*Moresi and Solomatov*, 1998] and regional studies [*Magee and Zoback*, 1993; *Wang et al.*, 1995]. Because of this low strength, it follows that the overriding plate is not the primary factor controlling the subduction velocity. Furthermore, a recent global statistical investigation indicates that the subducted slab predominantly determines the trench velocity, while the role of the overriding plate in determining the trench velocity is of subordinate importance [*Schellart*, 2008b]. As such, we argue that exclusion of an overriding plate is justified as a first-order approximation. Recent 3D numerical, fully dynamic, subduction models [*Clark et al.*, 2008; *Yamato et al.*, 2009] that include an overriding plate do show significant reduction in trench velocity, but these 3D simulations have an overriding plate that is fixed to the lateral sidewall of the modeling domain and side plates that are fully coupled to the subducting plate and overriding plate. Such model set-ups evidently place significant constraints on the subduction process and retard the trench velocity. Indeed, 2D numerical models from *Capitanio et al.* [2010] with fixed and free overriding plates show that trench motion is close to zero in case of a fixed and strong overriding plate, while a free overriding plate allows for trench retreat comparable to models without an overriding plate.

[10] Another simplification in the models is the usage of Cartesian geometry, which implies a flat Earth approximation. For the narrow subduction zone models this is of no great significance as curvature is small, but for models with W = 2000–7000 km curvature in spherical geometry is more significant (18°–63°). A recent modeling effort from *Morra et al.* [2010] shows numerical spherical subduction models with subduction zone widths of 3000 and 6000 km, and the subduction kinematics of these models agrees very well with those of our widest plates (3000–7000 km) with subduction accommodated mostly by plate motion and minor trench migration. Considering that even for the widest plates the spherical geometry models and Cartesian geometry models give very similar results, we argue that our simplification of using a Cartesian geometry does not have a significant influence on the model outcomes.

[11] We calculated the trench-normal subducting plate velocity ($v_{SP\perp}$, trenchward is positive), trench-normal trench migration velocity ($v_{T\perp}$, retreat, i.e., toward the subducting plate, is positive) and subduction partitioning ($v_{SP\perp}/v_{S\perp}$, where $v_{S\perp} = v_{SP\perp} + v_{T\perp}$) for the numerical models with progressive time for individual 200 km trench segments using the local trench-normal horizontal velocity vectors at the trench.

2.2. Kinematic Calculations

[12] For the natural data set, $v_{SP\perp}$, $v_{T\perp}$ and $v_{SP\perp}/v_{S\perp}$ were calculated for all 24 major subduction zones on Earth (Figure 2). We use the convention that trenchward subducting plate motion and retrograde (oceanward, so toward the subduction plate side) trench motion (i.e., trench retreat) are positive. With these conventions, then $0 < v_{SP\perp}/v_{S\perp} < 1$ with both trenchward subducting plate motion and trench retreat, $v_{SP\perp}/v_{S\perp} > 1$ with trenchward subducting plate motion and trench advance (i.e., trench motion toward the overriding plate), and $v_{SP\perp}/v_{S\perp} < 0$ with oceanward subducting plate motion and trench retreat. The trench velocity was calculated as follows:

$$v_{T\perp} = v_{OP\perp} + v_{OPD\perp} + v_{A\perp} \quad (2)$$

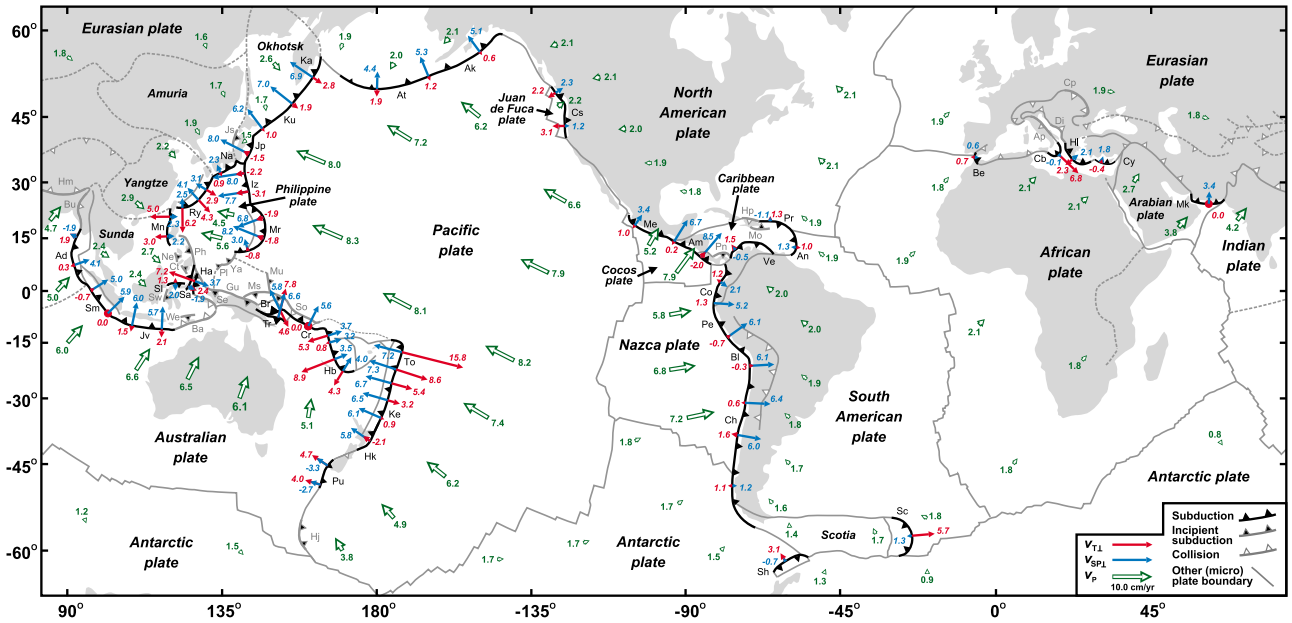

Figure 2. Global map illustrating the major subduction zones on Earth for which the trench-normal subducting plate velocity ($v_{SP\perp}$) and the trench-normal trench migration velocity ($v_{T\perp}$) have been plotted. Blue vectors illustrate $v_{SP\perp}$, red vectors illustrate $v_{T\perp}$, while large white vectors with green outline illustrate plate velocity (v_P) for the major plates and some microplates. Velocities were calculated in the Indo-Atlantic hot spot reference frame from *O'Neill et al.* [2005] using the geophysical relative plate motion model from *DeMets et al.* [1994] for motion of the major plates and using numerous microplate motions and backarc/arc/fore-arc deformation rates from other sources as summarized by *Schellart et al.* [2008, Tables 1 and 3] and *Schellart* [2008c, Tables S1 and S2]. Abbreviations for subduction zones/segments included in this study (included in Figures 5 and 6): Ad–Andaman, Ak–Alaska, Am–Central America, At–Aleutian, Bl–Bolivia, Br–New Britain, Cb–Calabria, Ch–Chile, Co–Colombia, Cr–San Cristobal, Cs–Cascadia, Ha–Halmahera, Hb–New Hebrides, Hk–Hikurangi, Hl–Hellenic, Iz–Izu-Bonin, Jp–Japan, Jv–Java, Ka–Kamchatka, Ke–Kermadec, Ku–Kuril, Me–Mexico, Mk–Makran, Mn–Manila, Mr–Mariana, Na–Nankai, Pe–Peru, Ry–Ryukyu, Sc–Scotia, Sh–South Shetland, Sl–North Sulawesi, Sm–Sumatra, To–Tonga. Abbreviations for subduction zones/segments not included in this study: An–Lesser Antilles, Be–Betic-Rif, Cy–Cyprus, Pr–Puerto Rico, Pu–Puysegur, Sa–Sangihe, Tr–Trobriand, Ve–Venezuela. Incipient subduction zones (also not included in this study): Ct–Cotobato, Gu–New Guinea, Hj–Hjort, Js–Japan Sea, Mo–Muertos, Ms–Manus, Mu–Mussau, Ne–Negros, Ph–Philippine, Pl–Palau, Pn–Panama, Sw–West Sulawesi, We–Wetar, Ya–Yap. Collision zones (also not included in this study): Ba–Banda, Bu–Burma, Cp–Carpathian, Di–Dinaride, Hm–Himalayas, Hp–Hispaniola, Se–Seram, So–Solomon.

where $v_{OP\perp}$ is the trench-normal overriding plate (+potential microplate) velocity (trenchward velocity is positive), $v_{OPD\perp}$ is the trench-normal overriding plate deformation rate (i.e., backarc/arc/fore-arc extension/spreading/shortening; extension/spreading is positive, shortening is negative), and $v_{A\perp}$ is the trench-normal trench accretion/erosion rate (accretion is positive, erosion is negative). Note that the subduction velocity $v_{S\perp} = v_{SP\perp} + v_{T\perp}$. Details on all the individual plates, microplates and backarc/arc/fore-arc deformation rates that have been used to calculate $v_{T\perp}$, and on all the individual plates and microplates to calculate $v_{SP\perp}$, are presented by *Schellart et al.* [2008, Tables 1 and 3] and *Schellart* [2008c, Tables S1 and S2]. Trench accretion/erosion rates for individual subduction zones were derived from *Clift and Vannucchi* [2004, and references therein], while a large number of microplate motions and backarc deformation rates were derived from *Kreemer et al.* [2003] and *Bird* [2003]. Additional sources on backarc/arc/fore-arc deformation rates and on motions of the microplates include *Zellmer and Taylor* [2001], *Darby and Meertens* [1995], *Wright* [1993], *Tregoning et al.* [1998, 1999], *Taylor et al.* [1995], *Calmant et al.* [1997], *Rangin et al.* [1999], *Nishimura et al.* [2004], *Mazzotti et al.* [2001], *Kozhurin et al.* [2006], *Seno et al.* [1993], *Wells et al.* [1998], *Suter et al.* [2001], *Norabuena et al.* [1998], *Thomas et al.* [2003], *Lawver et al.* [1995], *Nilforoushan et al.* [2003], *Gutscher et al.* [2002], *Rosenbaum and Lister* [2004], and *McClusky et al.* [2000].

[13] Each of the 24 subduction zones was subdivided into 200 km trench segments (total of 244 segments). The size of the trench segments was based on the rationale that it should be more than the thickness of mature oceanic lithosphere (~100 km) but should not exceed the width of the narrowest slabs (~300 km). Subduction zone segments for which the subduction velocity $v_{S\perp} \leq 1.5$ cm/yr, as well as all segments of a particular subduction zone for which the average $v_{S\perp} \leq 1.5$ cm/yr or for which at least half the segments have $v_{S\perp} \leq 1.5$ cm/yr, were excluded from the calculations, because

small fluctuations in $v_{SP\perp}$ or $v_{T\perp}$ at such low velocities (e.g., due to possible errors of only a few mm/yr or due to variation in the velocities due to the choice of global reference frame) dramatically alter $v_{SP\perp}/v_{S\perp}$. Due to this exclusion criterion, results for 17 subduction zones (with a total of 207 trench segments) are presented rather than for 24 zones.

[14] Plate velocities and plate boundary velocities depend on the choice of global reference frame. We use the Indo-Atlantic moving hot spot reference frame [*O'Neill et al.*, 2005] as our preferred frame of choice, because in this reference frame subduction partitioning ratios are most in agreement with the observed geometry of upper mantle and transition zone slabs [*Schellart*, 2011]. Also, in this reference frame viscous dissipation in the upper mantle is minimized, trenches predominantly retreat, and subducting plates mostly move trenchward (see *Schellart et al.* [2008] for more discussion). We combine this reference frame with the geophysical relative plate motion model from *DeMets et al.* [1994] for the motions of the major plates. We also present results in three other global reference frames to demonstrate that our main findings and conclusions are not dependent on the choice of reference frame. One of these additional reference frames is the no-net-rotation reference frame from *DeMets et al.* [1994]. The other two are the Pacific hot spot reference frame from *Wessel et al.* [2006] and the Antarctic plate reference frame from *Hamilton* [2003], which are also combined with the geophysical relative plate motion model from *DeMets et al.* [1994].

[15] For the nature-model comparison (see section 3.2) the velocities for both nature and models were averaged for individual 200 km trench segments. For the numerical models, the velocities were averaged for 4 Ma periods. Data for the first 8 Ma were excluded, as this period includes the incipient subduction stage during which the slab is mostly steepening, the subduction velocities are slower and the average slab length is relatively short (300–350 km), i.e., slower and shorter than for most of the 17 natural subduction zones presented here. The natural subduction zones that are included in this study are in different stages of their evolution. For some the slab tip has reached a depth of ~500–600 km (e.g., Aleutians, Ryukyu, New Hebrides, New Britain), for others it has just reached the transition zone (~660 km, e.g., Scotia), for some the slab lies on the transition zone (e.g., Tonga, Japan, Izu-Bonin, Calabria), and for some the slab penetrates into the lower mantle (e.g., Hellenic, Mariana, Central America, Cascadia, Sumatra-Java). As such, all the different natural subduction zones and their segments show the range of subduction zone evolution that is replicated in the models, and a comparison as presented in section 3.2 is therefore justified. The choice of averaging the model velocity data for 4 Ma periods is based on the time period for which the relative plate motions are averaged, which is 3.2 Ma for the *DeMets et al.* [1994] relative plate motion model.

3. Results

3.1. General Results of Subduction Models

[16] A total of 11 models were run with different slab widths (W = 300–7000 km). In all models subducting plate motion is always directed trenchward due to trenchward pull from the slab. The subduction models can be subdivided into three main subduction categories that are defined by similar subduction kinematics and a similar geometrical evolution [*Schellart et al.*, 2007]: narrow slab models (W = 300–1500 km), intermediate width slab models (W = 2000–3000 km) and wide slab models (W = 4000–7000 km). Below the general model results will be discussed for a narrow slab model (W = 300 km) and a wide slab model (W = 7000 km). Figure 3 shows the general evolution of these two models.

[17] The narrow slab model with W = 300 km shows subduction with backward sinking of the slab, trench retreat and progressive draping of the slab on top of the upper-lower mantle discontinuity (Figures 3a–3c). In general, narrow slab models (W = 300–1500 km) show broadly the same subduction evolution pattern. Subduction is characterized by rapid trench retreat, slow trenchward plate motion and low partitioning with $v_{SP\perp}/v_{S\perp}$ = 0.2–0.4 (Figure 4), except for the earliest subduction stage. In this early stage (0–5 million years) the slab is predominantly steepening, the slab tip is relatively shallow (~150–380 km deep) and subduction velocities are low (<2 cm/yr). The narrow slab models also show a progressive development of a curved slab and a curved trench that are concave toward the mantle wedge, as reported earlier for subduction zones with a width of ~300–1500 km [*Morra et al.*, 2006; *Schellart et al.*, 2007; *Schellart*, 2004, 2010].

[18] The wide slab model with W = 7000 km shows progressive subduction that is dominated by a relatively stable trench in the central part of the subduction zone and development of a folded slab pile at the 660 km discontinuity, but near the lateral slab edges moderate trench retreat occurs with backward sinking of the slab and minor draping of the slab on top of the upper-lower mantle discontinuity (Figures 3d–3f). In general, wide slab models (W = 4000–7000 km) show broadly the same subduction evolution pattern. Subduction is characterized by overall slow trench migration, rapid trenchward plate motion and high partitioning with $v_{SP\perp}/v_{S\perp}$ = 0.7–1.2 (Figure 4), except for the earliest stage (before ~7 million years). These models also show a progressive development of a curved subduction zone that is overall convex toward the mantle wedge but has concave edges, as reported earlier [*Schellart et al.*, 2007; *OzBench et al.*, 2008].

[19] The models with an intermediate slab width (W = 2000–3000 km) show intermediate behavior with some slab draping on top of the 660 km discontinuity but also formation of recumbent slab folds, and intermediate values for $v_{SP\perp}$ and $v_{T\perp}$. The change in subduction behavior from narrow to intermediate width slabs at ~1500–2000 km and then to wide-slab behavior is potentially related to the depth of the upper mantle (~660 km) and the length scale of the quasi-toroidal return flow that results from lateral migration of the slab through the upper mantle during rollback and roll-forward. The plan view geometry of this toroidal-type flow pattern is roughly circular and the radius of this flow pattern scales roughly with the half width of the slab [*Schellart et al.*, 2010].

[20] Figure 4 shows $v_{SP\perp}$, $v_{T\perp}$, $v_{S\perp}$ and $v_{SP\perp}/v_{S\perp}$ for the two simulations as measured in the center of the subduction zone, and as measured near the slab edge for the wide slab model (D_{SE} = 300 km). The two models show trenchward plate motion throughout the experiment as indicated by their

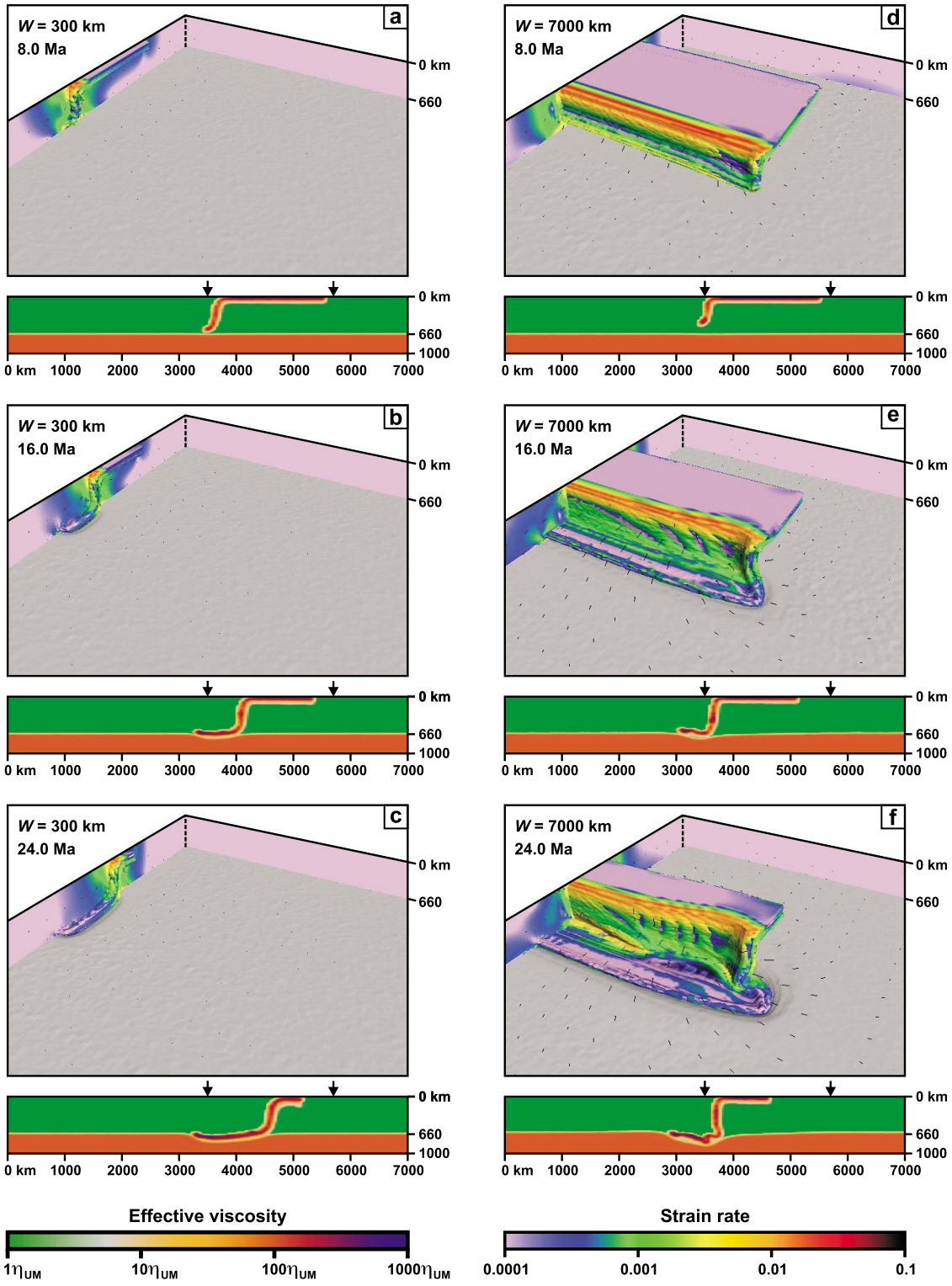

Figure 3. Three-dimensional perspective views and cross-sections showing three evolutionary stages of subduction in two subduction models. (a–c) Narrow slab model (W = 300 km). (d–f) Wide slab model (W = 7000 km). Three-dimensional views show strain rate (with highest strain rate at the trench) and cross-sections show viscosity. Note the negligible strain rates at the back wall and in the trailing plate. Cross-sections are from the center of the subduction zone (symmetry plane in Figure 1b). Arrows in cross-sections show location of trench (left) and trailing edge (right) at the start of each experiment.

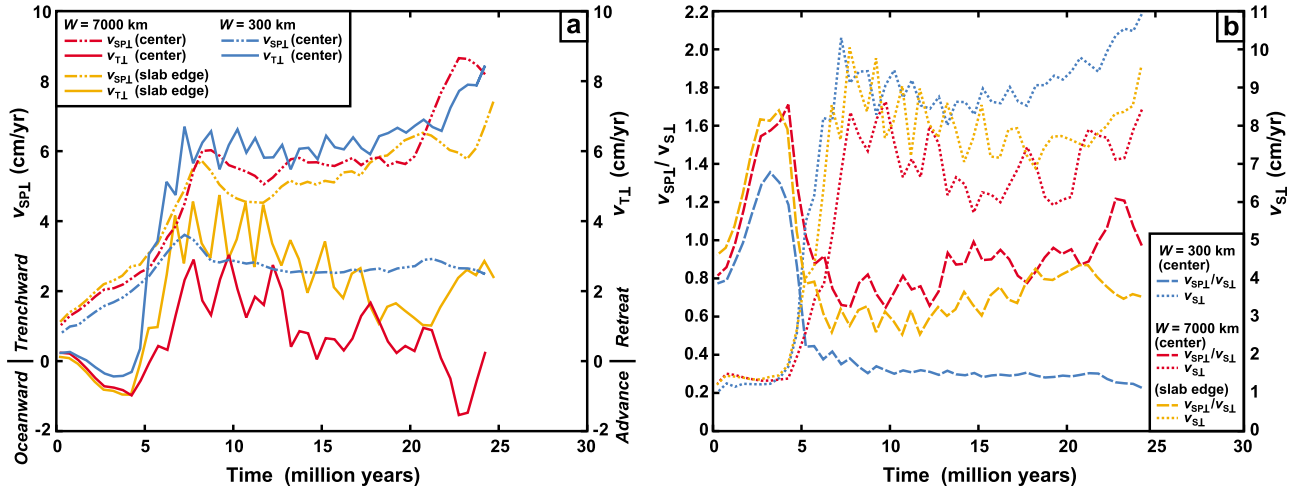

Figure 4. Diagrams showing the progressive development of (a) the trench-normal subducting plate velocity ($v_{SP\perp}$) and trench-normal trench velocity ($v_{T\perp}$); and (b) the subduction partitioning ratio ($v_{SP\perp}/v_{S\perp}$) and the subduction velocity ($v_{S\perp}$) for two subduction simulations with a slab width W = 300 km and W = 7000 km. For the narrow slab model the velocities and partitioning ratio are measured in the center of the subduction zone, while for the wide slab model the velocities and partitioning ratio are measured in the center of the subduction zone as well as close to the lateral slab edge (D_{SE} = 300 km).

positive $v_{SP\perp}$ values. In the center the models show a progressive increase in $v_{SP\perp}$ until a maximum of 3.5 cm/yr at ~7.2 million years for the narrow slab and a local maximum of 6.0 cm/yr at ~8.5 million years for the wide slab. There is also an increase in $v_{T\perp}$ until local maxima of 6.7 cm/yr (W = 300 km) and 2.9 cm/yr (W = 7000 km) are reached at approximately the same time. At this time the slab tip approaches the 660 km discontinuity with a slab tip depth of 580 km (W = 300 km) and 550 km (W = 7000 km; note that near the edges the slab has already reached the discontinuity). The viscosity step at the discontinuity slows down the sinking of the slab, as shown by the general decrease in $v_{S\perp}$ (Figure 4b), and forces the slab to bend here. After the maximum, $v_{SP\perp}$ and $v_{T\perp}$ decrease briefly for W = 300 km and then enter a relatively steady state of 2.5–2.9 cm/yr and 5.5–8.4 cm/yr respectively. For W = 7000 km $v_{SP\perp}$ and $v_{T\perp}$ decrease briefly and then vary within a relatively broad range of 5.1–8.7 cm/yr and −1.5 to 3.0 cm/yr respectively.

[21] Figure 4b shows that the narrow slab is subducting faster than the wide slab. This can be ascribed to the fact that the narrow slab experiences relatively minor resistance to lateral migration of the upper mantle slab and trench retreat, while the central segment of the wide slab experiences considerable resistance from the ambient mantle to lateral slab migration and trench retreat. As such, in the models, which have no tearing resistance at the slab edges, narrow slabs subduct more efficiently than central segments of wide slabs. In a similar way, segments of the wide slab close to the lateral slab edges (small D_{SE}) subduct faster than the central segment (large D_{SE}), as demonstrated by the $v_{S\perp}$ curves in Figure 4b.

3.2. Subduction Dependence on D_{SE}

[22] From the global map in Figure 2 and the global kinematic data set in Figures 5a–5c it can be observed that variations in $v_{SP\perp}$, $v_{T\perp}$ and $v_{SP\perp}/v_{S\perp}$ on Earth are significant, with $v_{SP\perp}$ ranging from −1 to 9 cm/yr, $v_{T\perp}$ from −4 to 16 cm/yr, and $v_{SP\perp}/v_{S\perp}$ from −0.4 to 1.8 (Figures 5a–5c). The kinematic data for the natural subduction zones and the dynamic models (Figures 5d–5f) show a distribution that is not random with respect to the distance to the closest lateral slab edge (D_{SE}), but is limited to certain regions, indicating that D_{SE} affects subduction kinematics.

3.2.1. Trench-Normal Subducting Plate Velocity ($v_{SP\perp}$)

[23] Subducting plate motion is always fast far from lateral slab edges (D_{SE} > 2200 km) with $4.2 \le v_{SP\perp} \le 8.0$ cm/yr (nature) and $5.1 \le v_{SP\perp} \le 7.6$ cm/yr (models) (Figures 5a and 5d). Slow subducting plate velocities ($v_{SP\perp}$ < 2.0 cm/yr for nature and $v_{SP\perp}$ < 4.0 cm/yr for models) are only observed close to slab edges (D_{SE} < ~1000 km).

[24] For the models, the lowest $v_{SP\perp}$ are observed for narrow slabs. In nature, the lowest $v_{SP\perp}$ are also frequently observed for narrow slabs (e.g., Scotia, Hellenic, North Sulawesi, Manila), but a number of wide subduction zones also show a decrease toward either one or both slab edges (e.g., South America, Aleutians-Alaska, Kamchatka-Kuril-Japan-Izu-Bonin-Mariana, Sunda), and this decrease can be up to 5 cm/yr. This general pattern is replicated in the models, where the widest slabs (W = 5000–7000 km) consistently show a general decrease in $v_{SP\perp}$ toward the slab edges ranging from a few mm/yr up to 1.7 cm/yr.

[25] The mean and median $v_{SP\perp}$ in nature are 4.79 cm/yr and 5.34 cm/yr, respectively (Figure 5a). For most subduction zone segments the subducting plate moves trenchward (97% for nature and 100% for models), as would be expected for plate motion that is dominated by pull from negatively buoyant slabs.

3.2.2. Trench-Normal Trench Velocity ($v_{T\perp}$)

[26] Figures 5b and 5e show that trench retreat is always slow for D_{SE} > 2200 km with $v_{T\perp} \le 1.7$ cm/yr (nature) and $v_{T\perp} \le 2.5$ cm/yr (models), while fast trench retreat ($v_{T\perp}$ > 6.1 cm/yr (nature) and $v_{T\perp}$ > 4.0 cm/yr (models)) is only observed close to lateral slab edges (D_{SE} < 1000 km). These findings are in general agreement with previous findings for

natural subduction zones [*Schellart et al.*, 2007, 2008]. The mean and median $v_{T\perp}$ in nature are 1.47 cm/yr and 1.08 cm/yr, respectively, and 72.9% of the trench segments are in a retreating mode (Figure 5b).

[27] For the models, the highest $v_{T\perp}$ are observed for the narrowest slabs (W = 300–900 km with $v_{T\perp}$ = 5–7 cm/yr), while the widest slabs (W = 5000–7000 km) consistently show a general increase in $v_{T\perp}$ toward the slab edges (by 1.0–2.4 cm/yr). In nature, high $v_{T\perp}$ are also frequently observed for narrow slabs (e.g., Scotia, Calabria, Halmahera, Manila), but the two highest $v_{T\perp}$ are observed near the edges of two relatively wide slabs, namely the northern slab edge of the Tonga-Kermadec-Hikurangi subduction zone (W = 3550 km) and the southeastern slab edge of the Melanesian subduction zone (W = 4400 km), i.e., the southeast New Hebrides segment.

[28] It is worth noting that in the models the subduction segments with $D_{SE} \approx$ 0–600 km show a rapid decrease in $v_{T\perp}$ toward the slab edge. This is particularly evident for the models with W = 1200–7000 km. This is also observed for several subduction zone edges in nature, such as northern Tonga, southern New Hebrides, Scotia, southwestern Ryukyu and eastern Hellenic, but the length scale over which it occurs is somewhat shorter, with $D_{SE} \approx$ 0–400 km. Such rapid decrease can be ascribed entirely to the progressive development of plan view curvature (concave toward the mantle wedge) of the trench edge and the slab edge.

3.2.3. Subduction Partitioning ($v_{SP\perp}/v_{S\perp}$)

[29] Figures 5c and 5f show the natural data and model results for subduction partitioning. Note that when $v_{SP\perp}/v_{S\perp}$ = 0.5 subduction is equally partitioned between trenchward subducting plate motion and trench retreat. The

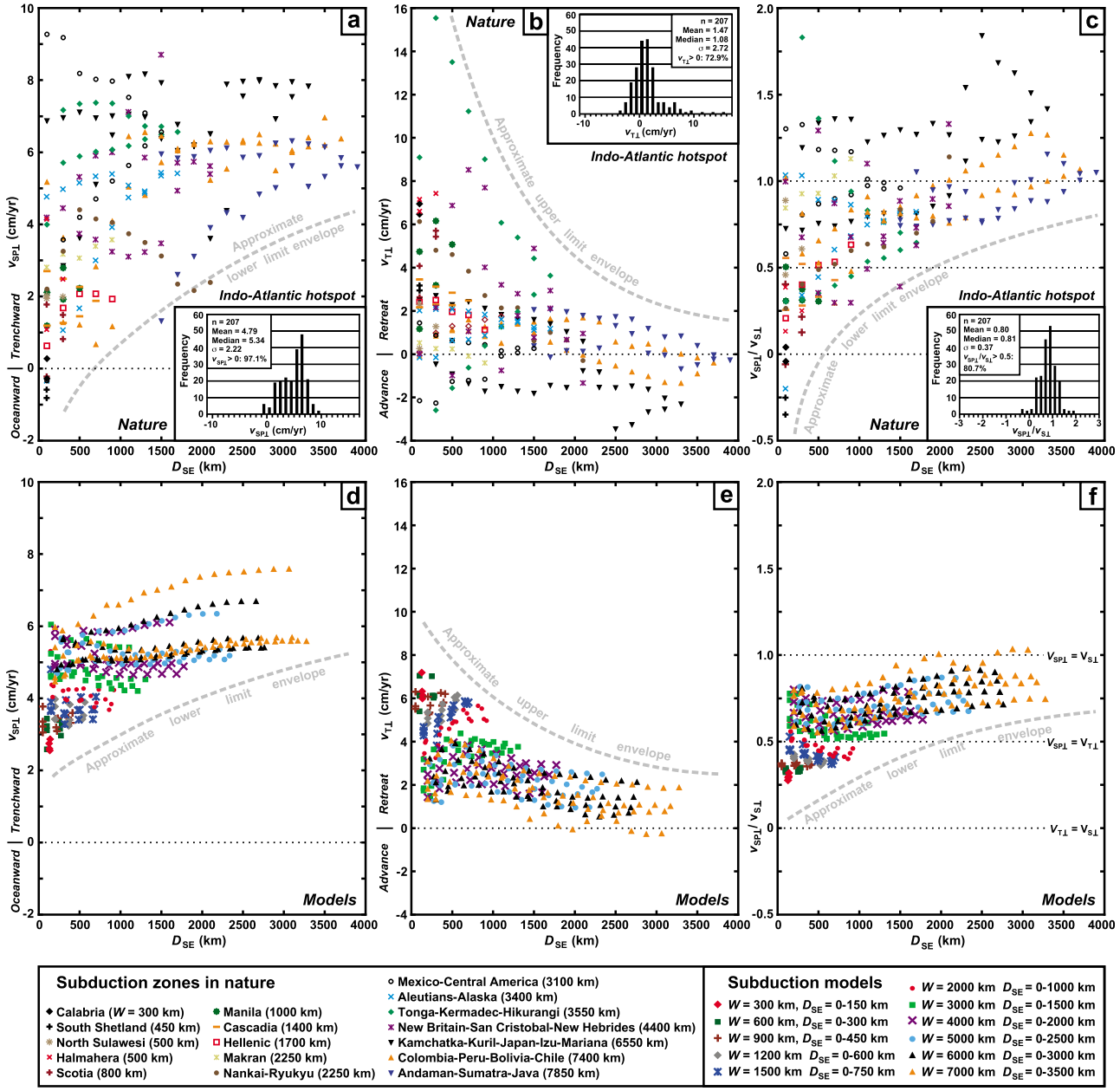

Figure 5

mean partitioning in nature is 0.80, the median partitioning is 0.81, while for 80.7% of the trench segments $v_{SP\perp}/v_{S\perp} > 0.5$. This indicates that on a global scale subduction is dominated by trenchward subducting plate motion, not trench retreat. Partitioning is always high far from slab edges (D_{SE} > 2200 km), with $0.76 \le v_{SP\perp}/v_{S\perp} \le 1.84$ (nature) and $0.68 \le v_{SP\perp}/v_{S\perp} \le 1.04$ (models). Low partitioning ratios in nature ($v_{SP\perp}/v_{S\perp} < 0.39$) and models ($v_{SP\perp}/v_{S\perp} < 0.52$) are only found close to lateral slab edges (D_{SE} < 1000 km).

[30] In the models, the lowest partitioning ratios are found for narrow slabs such as W = 300 km with $v_{SP\perp}/v_{S\perp}$ = 0.28–0.32 (Figure 5f). In nature, the lowest $v_{SP\perp}/v_{S\perp}$ are also mostly observed for narrow slabs (e.g., Scotia, Calabria, Halmahera), but a number of wide subduction zones also show a considerable decrease toward either one or both slab edges (e.g., South America, Aleutians-Alaska, Kamchatka to Mariana, Sunda). Such a general decrease in $v_{SP\perp}/v_{S\perp}$ toward the slab edges for wide slabs is replicated in the models, in particular those with W = 5000–7000 km. For example, for W = 7000 km, $v_{SP\perp}/v_{S\perp}$ = 0.75–1.03 when D_{SE} > 3000 km and $v_{SP\perp}/v_{S\perp}$ = 0.56–0.83 when D_{SE} < 1000 km (Figure 5f).

3.2.4. Results for Different Global Reference Frames

[31] Calculations in the other three reference frames, the no-net-rotation reference frame from *DeMets et al.* [1994], the Pacific hot spot reference frame from *Wessel et al.* [2006] and the Antarctic plate reference frame from *Hamilton* [2003] (Figure 6) show results that are similar to those in the Indo-Atlantic hot spot reference frame (Figures 5a–5c). The distribution of the data points in the different reference frames is similar, in particular for the Indo-Atlantic hot spot and the no-net-rotation reference frames. The results in the Pacific hot spot reference frame and the Antarctic plate reference frame are also very comparable to each other. In general, the four reference frames show that low $v_{SP\perp}$, high $v_{T\perp}$ and low $v_{SP\perp}/v_{S\perp}$ only occur in regions close to lateral slab edges. They further show that central regions of wide slabs always have high $v_{SP\perp}$, low $v_{T\perp}$ and high $v_{SP\perp}/v_{S\perp}$. The four reference frames further show that subduction zone trenches generally retreat (66.2–78.3%), that subducting plates mostly move trenchward (95.2–97.6%), and that subduction is predominantly accommodated by trenchward plate motion ($v_{SP\perp}/v_{S\perp} > 0.5$ for 75.4–80.7% of trench segments).

4. Discussion

4.1. Discussion of General Results

[32] Models and nature are in qualitative and quantitative agreement and they show that: (1) Low subducting plate velocities, high trench retreat velocities and low partitioning ratios are only found in regions close to lateral slab edges; (2) Central regions of wide slabs always have high subducting plate velocities, low trench retreat velocities and high partitioning ratios (Figure 5).

[33] The dependence of $v_{T\perp}$ on D_{SE} observed in models and nature is explained by the viscous drag that the upper mantle quasi-toroidal return flow experiences at the viscosity step at upper-lower mantle boundary during lateral slab migration. This viscous resistance scales with $\sim W^2$ because the planar projection of the quasi-toroidal return flow is roughly circular and its diameter scales with W. As the negative buoyancy of the slab scales with W, it follows that $v_{T\perp}$ roughly scales with $1/W$ [*Schellart et al.*, 2010]. Slab segments close to lateral slab edges will thus experience relatively minor resistance from the ambient mantle to migrate laterally because the plan view area of the required return flow pattern will be relatively small, resulting in relatively fast $v_{T\perp}$. In contrast, segments far from lateral slab edges will experience large resistance from the ambient mantle because the plan view area of the required return flow pattern will be relatively large, resulting in relatively slow $v_{T\perp}$. Because $v_{S\perp}$ is similar for narrow and wide slabs (Figure 4), it follows that a dependence of $v_{T\perp}$ on D_{SE} translates into a dependence of $v_{SP\perp}$ and $v_{SP\perp}/v_{S\perp}$ on D_{SE} (considering that $v_{S\perp} = v_{T\perp} + v_{SP\perp}$).

[34] For narrow slabs, each subduction segment is located close to a lateral slab edge, and therefore the whole slab can rapidly retreat (assuming that the slab can easily tear at its edges). Thus, trench retreat is efficient and is the preferred mode of subduction, at the expense of trenchward subducting plate motion. For wide slabs, only segments close to

Figure 5. Diagrams showing the influence of lateral slab edge proximity (D_{SE}) on subduction kinematics. Influence of D_{SE} on: (a and d), the trench-normal subducting plate velocity ($v_{SP\perp}$), (b and e), the trench-normal trench migration velocity ($v_{T\perp}$), and (c and f), the subduction partitioning ratio ($v_{SP\perp}/v_{S\perp} = v_{SP\perp}/(v_{SP\perp}+v_{T\perp})$). For Figures 5a–5c data are from 17 subduction zones on Earth and in Figures 5d–5f data are from 11 numerical models of progressive subduction in three-dimensional space. For nature and models, the subduction zones were segmented into 200 km segments (total of 207 segments for nature, ~41,400 km). Subduction zone widths are shown in the key. In nature, velocities were calculated in the Indo-Atlantic hot spot reference frame from *O'Neill et al.* [2005] using the geophysical relative plate motion model from *DeMets et al.* [1994] for motion of the major plates and using numerous microplate motions and backarc/arc/fore-arc deformation rates from other sources as summarized in *Schellart et al.* [2008, Tables 1 and 3] and *Schellart* [2008c] (his Tables S1 and S2). For the numerical models, data were extracted from eleven simulations with a different slab width (initial slab width W = 300–7000 km). Each simulation ran for 25–27 million years and data as shown in d–f were extracted from a 16 million year period by excluding the first 8 million years that are characterized by the initial (transient) subduction stage and excluding the last 1–3 million years that are characterized by the final (transient) subduction stage. For this 16 million year time span data were averaged for 4 million year periods, resulting in four data points for each trench segment in Figures 5d–5f. For $v_{SP\perp}/v_{S\perp} > 0.5$ and $v_{SP\perp}/v_{S\perp} < 0.5$ subduction is mainly due to trenchward subducting plate motion and trench retreat, respectively. Note that segments with $v_{S\perp} \le 1.5$ cm/yr, and subduction zones for which the average $v_{S\perp} \le 1.5$ cm/yr or for which at least half the segments had $v_{S\perp} \le 1.5$ cm/yr, were excluded from the calculations. Figure 5b is modified and updated from *Schellart et al.* [2007]. Thick gray dashed lines indicate approximate locations of lower limit envelopes or upper limit envelopes. Insets in a–c show frequency plots for $v_{SP\perp}$, $v_{T\perp}$ and $v_{SP\perp}/v_{S\perp}$.

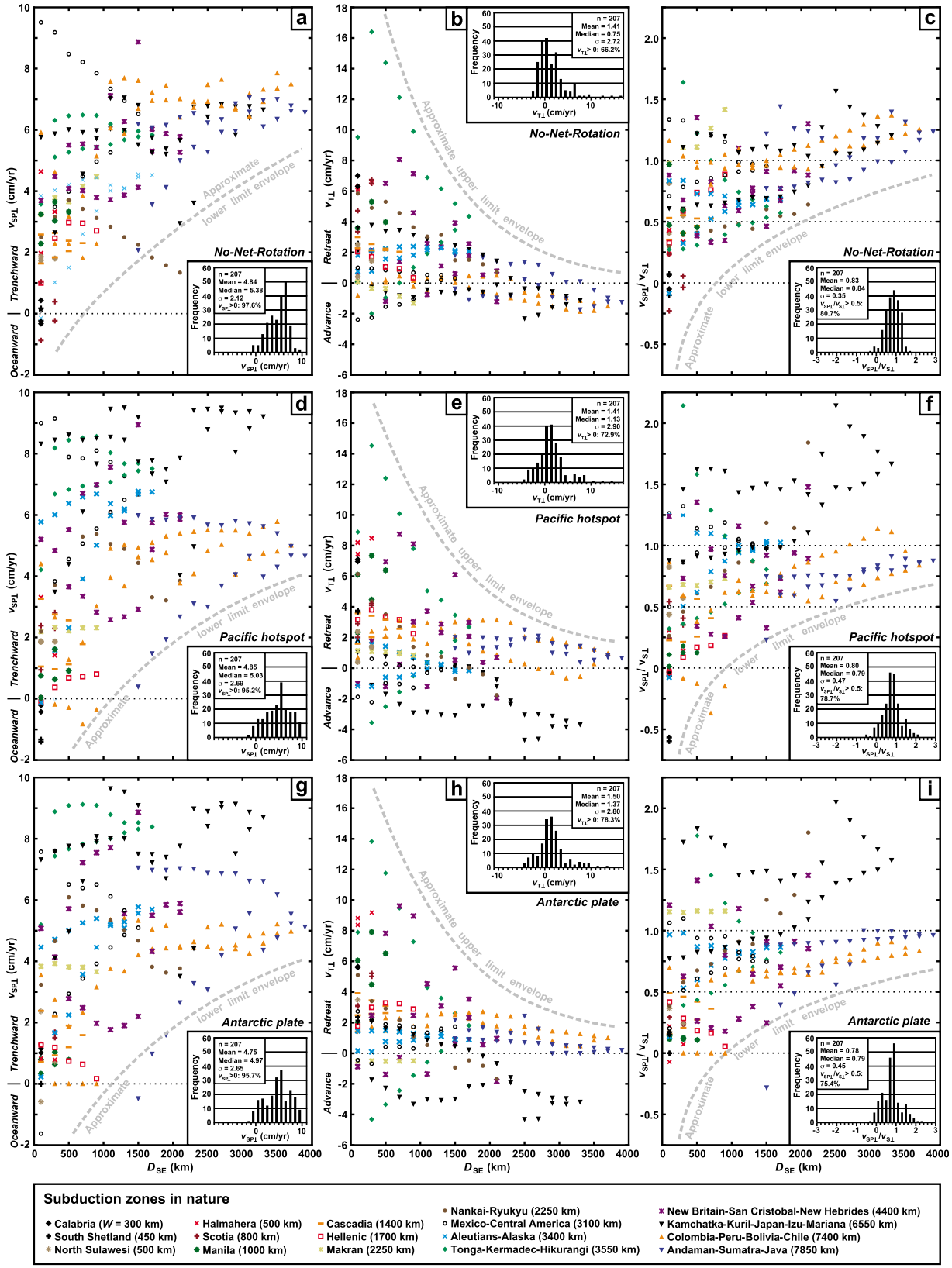
a
b
c
d
e
f
g
h
i
No-Net-Rotation
Pacific hotspot
Antarctic plate
Approximate upper limit envelope
Approximate lower limit envelope
Oceanward
Trenchward
Retreat
Advance
v_{SPL} (cm/yr)
v_{TL} (cm/yr)
v_{SPL}/v_{SL}
D_{SE} (km)
Frequency
Subduction zones in nature
Calabria (W = 300 km)
South Shetland (450 km)
North Sulawesi (500 km)
Halmahera (500 km)
Scotia (800 km)
Manila (1000 km)
Cascadia (1400 km)
Hellenic (1700 km)
Makran (2250 km)
Nankai-Ryukyu (2250 km)
Mexico-Central America (3100 km)
Aleutians-Alaska (3400 km)
Tonga-Kermadec-Hikurangi (3550 km)
New Britain-San Cristobal-New Hebrides (4400 km)
Kamchatka-Kuril-Japan-Izu-Mariana (6550 km)
Colombia-Peru-Bolivia-Chile (7400 km)
Andaman-Sumatra-Java (7850 km)

Figure 6

lateral slab edges can rapidly retreat (again, assuming that the slab can easily tear at its edges), while segments further away will show minor trench migration. Because slabs are relatively weak (~$10^2 \times \eta_{UM}$), wide slabs can accommodate such variation in slab rollback rate along the trench through internal plan view deformation and rotation. For wide slabs trench retreat is inefficient far from lateral slab edges, but becomes progressively more efficient close to the edges. As such, trenchward subducting plate motion is the preferred mode of subduction far from subduction zone edges, while the trench retreat mode of subduction becomes progressively more important closer to the edges.

4.2. Comparison Between Nature and Models

4.2.1. General Kinematics in Nature and Models

[35] The velocity distributions observed for $v_{SP\perp}$ and $v_{T\perp}$ in nature and models, as well as the partitioning ratios, are similar and the limiting envelopes have similar trends (Figure 5). The considerable spread in $v_{SP\perp}$, $v_{T\perp}$ and $v_{SP\perp}/v_{S\perp}$ in the numerical models is related to the temporal variability for individual subduction models (Figures 4 and 5d–5f). The temporal variability is particularly evident for the wide slab models, which results from the episodic phases of slab folding and draping on top of the 660 km discontinuity and the complex slab-mantle interaction and the lateral deformation of the slab. The spread in data for the natural subduction zones can be partly explained by such temporal variability, as the individual subduction zones in nature are in different stages of their evolution.

[36] Figure 5 further shows that the scatter of the velocities and $v_{SP\perp}/v_{S\perp}$ in nature is larger than that in the models. The larger scatter in the natural data is likely attributable to a variety of things, including inhomogeneities of subducting plates in nature (e.g., local subduction of plateaus or aseismic ridges; trench-parallel gradients in oceanic lithosphere age) [e.g., *Mason et al.*, 2010; *Morra et al.*, 2006], variation in size of the subducting plate that is independent of the size of the subduction zone, regional mantle flow patterns, variations in slab-plate tearing resistance at subduction zone edges [e.g., *Hale et al.*, 2010], overriding plate influence [e.g., *Capitanio et al.*, 2010; *van Dinther et al.*, 2010], and other factors not incorporated in the numerical models. For example, rapid trench advance ($v_{T\perp} < -1$ cm/yr) is not observed in the models for prolonged periods of time (≥3 million years). Thus, the relatively rapid trench advance for the Izu-Bonin-Mariana subduction section (−3 to −1 cm/yr) is most likely a combination of the large width of the entire subduction zone (~6550 km from Kamchatka to Mariana), the rapid westward motion of the overriding Philippine plate, ridge-push forces from the East Pacific Rise and the local indentation and subduction of the Ogasawara Plateau and Caroline Ridge at the trench. Three-dimensional subduction models indeed imply that local subduction of buoyant ridges or plateaus promotes trench advance [*Mason et al.*, 2010]. Very low subducting plate velocities (−1 to 1 cm/yr) observed for some subduction zones such as Hellenic, Calabria, Scotia and South Shetland are not observed in the numerical models, but could be explained by the combination of a very narrow slab and the fact that these slabs are attached to very large plates (i.e., Africa, South America and Antarctica), plates that are much larger than in the models, which would promote a reduction in $v_{SP\perp}$ due to the large total mantle drag force at the base of these plates.

4.2.2. Dependence on D_{SE} in Nature and Models

[37] The numerical models show that the lowest $v_{SP\perp}$ and $v_{SP\perp}/v_{S\perp}$ and the highest $v_{T\perp}$ are observed for narrow slabs, while the highest $v_{SP\perp}$ and $v_{SP\perp}/v_{S\perp}$ and the lowest $v_{T\perp}$ are observed for wide slabs (Figures 5d–5f). The widest slabs (W = 5000–7000 km) are characterized by a general decrease in $v_{SP\perp}$ (by 0.1–1.7 cm/yr) and $v_{SP\perp}/v_{S\perp}$ (by 0.10–0.27), and an increase in $v_{T\perp}$ (by 1.0–2.4 cm/yr), toward the slab edges. It should be emphasized that the decrease in $v_{SP\perp}$ would be even more pronounced in case the models would be run in spherical geometry, as trench segments close to the slab edges would be located closer to the Euler poles than central trench segments. For example, for a 7000 km wide plate this would mean an additional 15% reduction in $v_{SP\perp}$ at the edges compared to $v_{SP\perp}$ in the center.

[38] The results from the model with W = 7000 km best illustrate the dependence of $v_{SP\perp}$, $v_{T\perp}$ and $v_{SP\perp}/v_{S\perp}$ on D_{SE}. For the four time periods plotted in Figure 5d, the first two (8–16 Ma) show a moderate decrease from $v_{SP\perp}$ = ~5.5 cm/yr to ~4.5 cm/yr, the third (16–20 Ma) decreases slightly with an average around 5.5 cm/yr, and the last one (20–24 Ma) shows a clear decrease from 7.6 cm/yr at D_{SE} = 3060 km to 5.9 cm/yr at D_{SE} = 290 km. For the same model, $v_{T\perp}$ increases along the trench toward the slab edge (Figure 5e) from $v_{T\perp}$ = 1.9 to 4.1 cm/yr (8–12 Ma), 1.0 to 3.4 cm/yr (12–16 Ma), 0.7 to 2.6 cm/yr (16–20 Ma) and −0.3 to 1.8 cm/yr (20–24 Ma), while $v_{SP\perp}/v_{S\perp}$ decreases (Figure 5f) from 0.75 to 0.56 (8–12 Ma), 0.84 to 0.60 (12–16 Ma),

Figure 6. Diagrams showing the influence of lateral slab edge proximity (D_{SE}) on subduction kinematics for 17 active subduction zones on Earth in three global reference frames. Influence of D_{SE} on: (a, d, and g), the trench-normal subducting plate velocity ($v_{SP\perp}$), (b, e, and h), the trench-normal trench migration velocity ($v_{T\perp}$), and (c, f, and i), the subduction partitioning ratio ($v_{SP\perp}/v_{S\perp} = v_{SP\perp}/(v_{SP\perp} + v_{T\perp})$). In Figures 6a–6c data have been calculated using the *DeMets et al.* [1994] no-net-rotation reference frame, in Figures 6d–6f data have been calculated using the Pacific hot spot reference frame from *Wessel et al.* [2006] using the geophysical relative plate motion model from *DeMets et al.* [1994], and in Figures 6g–6i data have been calculated using the Antarctic plate reference frame from *Hamilton* [2003] using the geophysical relative plate motion model from *DeMets et al.* [1994]. The motions of numerous microplates and numerous backarc/arc/fore-arc deformation rates were included in this study and were derived from other sources as summarized by *Schellart et al.* [2008, Tables 1 and 3] and *Schellart* [2008c, Tables S1 and S2]. The subduction zones were segmented into 200 km segments (total of 207 segments for nature, ~41,400 km). Subduction zone widths are shown in the key. Note that segments with $v_{S\perp} \leq 1.5$ cm/yr, and subduction zones for which the average $v_{S\perp} \leq 1.5$ cm/yr or for which at least half the segments had $v_{S\perp} \leq 1.5$ cm/yr, were excluded from the calculations. Figures 6e and 6h are modified from *Schellart et al.* [2008]. Thick gray dashed lines indicate approximate locations of lower limit envelopes or upper limit envelopes. Insets show frequency plots for $v_{SP\perp}$, $v_{T\perp}$ and $v_{SP\perp}/v_{S\perp}$.

0.89 to 0.68 (16–20 Ma) and 1.04 to 0.77 (20–24 Ma). The model with W = 7000 km thus illustrates that $v_{SP\perp}$, $v_{T\perp}$ and $v_{SP\perp}/v_{S\perp}$ for wide slabs vary in space (i.e., dependence on D_{SE}) but also vary with time.

[39] The current data set for natural subduction zones is not suitable for resolving temporal variability, but the data set does show a spatial variability along individual subduction zones. Indeed, several wide subduction zones show a general decrease in $v_{SP\perp}$ and $v_{SP\perp}/v_{S\perp}$ and a general increase in $v_{T\perp}$ toward either one or both slab edges. One example is the South American subduction zone, which has high $v_{SP\perp}$ (6.0–7.0 cm/yr), low $v_{T\perp}$ (−1.3 to 0.2 cm/yr) and high $v_{SP\perp}/v_{S\perp}$ (0.97–1.28) at D_{SE} > 3000 km, and a lower $v_{SP\perp}$ (0.7–5.1 cm/yr), higher $v_{T\perp}$ (−0.1 to 1.6 cm/yr) and lower $v_{SP\perp}/v_{S\perp}$ (0.30–1.02) at D_{SE} < 1000 km. Other examples are Kamchatka-Kuril-Japan-Izu-Bonin-Mariana, Sunda and Aleutians-Alaska. For each of these three subduction zones, one slab edge region shows a much more significant decrease in $v_{SP\perp}$ than the other half, showing a clear departure from symmetrical kinematic behavior, which is obviously not replicated in the (symmetrical) numerical models. Such asymmetry could be ascribed to inhomogeneities on the subducting plate, such as subduction of a buoyant aseismic ridge or plateau, or a trench-parallel gradient in subducting plate age. An asymmetry in subducting plate age (increasing southeastward) and subduction of an aseismic ridge (Cocos ridge) might also explain the rapid increase in subducting plate velocity and decrease in trench velocity from the northwestern edge of the Mexico-Central America subduction zone toward its southeastern edge (Figures 5a–5b).

[40] The highest trench retreat velocities, observed for Northern Tonga and southern New Hebrides (~8–16 cm/yr), are not reproduced in the models. The highest trench retreat velocities of 7–8 cm/yr are observed for the narrow slab models (W = 300–600 km). The wide slab model (W = 4000 km) that is comparable to Tonga-Kermadec-Hikurangi (W = 3550 km) and Melanesia (W = 4400 km) has a maximum trench retreat velocity of 4 cm/yr close to its slab edges. Thus, one might need to invoke other mechanisms that contribute to the rapid trench retreat in these two tectonic settings. For Tonga-Kermadec-Hikurangi one mechanisms might be the collision of the Chatham rise and the subduction of the buoyant Hikurangi plateau in the south, which enhances trench advance in this region (which is indeed observed), inducing toroidal flow patterns from the Hikurangi mantle wedge region toward the Tonga mantle wedge region, thereby providing an additional push to the Tonga slab and thus facilitating rapid slab rollback and trench retreat. It is worth noting that when the trench velocities for Tonga-Kermadec-Hikurangi and Melanesia are ignored in Figure 5b, then the upper limit envelope for the natural data set would be nearly identical to that for the models in Figure 5e.

4.3. Subduction Zones Excluded From the Calculations

[41] The results presented in Figures 5a–5c and 6 do not include subduction zones with slow average subduction rates (≤1.5 cm/yr) or subduction zones for which at least half the trench segments have $v_{S\perp} \leq 1.5$ cm/yr, i.e., Venezuela, Lesser Antilles, Cyprus, Puysegur, Betic-Rif, Trobriand and Sangihe. This is because at such low subduction velocities, small changes in $v_{SP\perp}$ or $v_{T\perp}$ (due to uncertainties or choice of reference frame) will have a dramatic effect on subduction partitioning. These subduction zones are all relatively narrow (W = 250–2450 km) and would thus only populate the region close to lateral slab edges (D_{SE} = 0–1225 km). As such, exclusion of these data has no impact on the conclusions drawn for the behavior of centers of wide subduction zones. In regards to the behavior of subduction zones near lateral slab edges, exclusion of the seven subduction zones does not affect the main conclusions. For these subduction zones $v_{SP\perp}$ = −6.7 to 1.9 cm/yr, $v_{T\perp}$ = −0.3 to 7.7 cm/yr and $v_{SP\perp}/v_{S\perp}$ = −96 to 2.9 (in the Indo-Atlantic hot spot reference frame). The range of $v_{T\perp}$ values for the seven zones falls within the wider range observed in Figure 5b, indicating that exclusion of these data has no effect on the overall distribution pattern of the data. Significant negative $v_{SP\perp}$ and $v_{SP\perp}/v_{S\perp}$ values are found only for Puysegur, Trobriand and Venezuela, suggesting that these subduction zones are not yet self-sustaining, i.e., not driven primarily by their own negative buoyancy. This appears plausible, because the slabs at these subduction zones have only reached a depth of about 150–300 km, as implied by their Wadati-Benioff zone and tomographic imaging [*Cooper and Taylor*, 1987; *van der Hilst and Mann*, 1994; *Lebrun et al.*, 2000; *Hall and Spakman*, 2002]. Because of the likelihood that these subduction zones are not driven primarily by their own negative buoyancy, comparison with the numerical model results is unwarranted, considering that in the models subduction is driven entirely by the negative buoyancy force of the slab.

4.4. Comparison With Previous Modeling

[42] The general subduction evolution of the models is similar to previous laboratory and numerical models of progressive subduction in three-dimensional space that use a similar (low) slab to upper mantle effective viscosity ratio ($\eta_{SP}/\eta_{UM} \approx 10^2$). Earlier narrow-slab models also showed rapid trench retreat and a trench curvature that is concave toward the mantle wedge [e.g., *Stegman et al.*, 2006; *Morra et al.*, 2006; *Schellart*, 2004, 2010; *Schellart et al.*, 2007], and wide-slab models also showed slow trench migration and an overall convex trench geometry with concave edges [*Schellart et al.*, 2007; *OzBench et al.*, 2008; *Stegman et al.*, 2010b].

[43] *Schellart et al.* [2010] demonstrated the important control of slab width on average $v_{SP\perp}$, $v_{T\perp}$ and $v_{SP\perp}/v_{S\perp}$ for individual subduction zones. The results presented here agree with these general findings but add to this that the variation of subduction zone behavior along individual subduction zones can be understood to a large extent when taking into consideration the presence of lateral slab edges and the distance of individual trench segments to their closest lateral slab edge.

[44] Previous three-dimensional dynamic models of progressive free subduction of narrow slabs ($W \leq 1500$ km) with low η_{SP}/η_{UM} values of $1–2 \times 10^2$ (as here) only showed low partitioning ratios of $v_{SP\perp}/v_{S\perp}$ = 0.1–0.5 [*Schellart*, 2004, 2008a; *Stegman et al.*, 2006], in agreement with the results presented here for narrow slabs. Higher partitioning ratios ($v_{SP\perp}/v_{S\perp} > 0.5$) have previously only been observed for fully dynamic subduction models when high values of η_{SP}/η_{UM} (≥1000) were adopted [*Faccenna et al.*, 2007;

Di Giuseppe et al., 2008; *Schellart*, 2008a; *Stegman et al.*, 2010a]. One could thus argue that in nature η_{SP}/η_{UM} must be high, at least for those subduction zones where $v_{SP\perp}/v_{S\perp}$ is high (e.g., Kamchatka-Kuril-Japan-Izu-Bonin-Mariana, Aleutians-Alaska, Sunda). However, the results presented in here (Figure 5) show that such high partitioning ratios can be reproduced in fully dynamic models with low η_{SP}/η_{UM} values ($1–2 \times 10^2$) when effects due to variations in slab width and lateral slab edge proximity are accounted for. In the center of wide slabs, far away from lateral slab edges ($D_{SE} > 2200$ km), partitioning is always high (0.68–1.04, Figure 5f).

5. Conclusions

[45] We have presented results of subducting plate velocity, trench velocity and subduction partitioning for 17 active natural subduction zones and for 11 numerical models of progressive subduction in three-dimensional space. Models and nature are in qualitative and quantitative agreement with regards to the dependence of subduction kinematics on slab edge proximity (Figure 5). Most importantly, far from lateral slab edges (i.e., in the center of wide subduction zones) $v_{SP\perp}$ is always fast, $v_{T\perp}$ is always slow and $v_{SP\perp}/v_{S\perp}$ is always high. Furthermore, slow $v_{SP\perp}$, fast $v_{T\perp}$ and low $v_{SP\perp}/v_{S\perp}$ are only observed close to lateral slab edges. As is evident from Figure 5, this does not mean that $v_{SP\perp}$ is always slow, $v_{T\perp}$ is always fast and $v_{SP\perp}/v_{S\perp}$ is always low in regions close to lateral slab edges, because of the dependence of the velocity parameters on other physical parameters such as slab length, slab resistance to tearing and subduction of buoyant features such as aseismic ridges and plateaus. It does mean, however, that lateral slab edge proximity is a requirement for slow $v_{SP\perp}$, fast $v_{T\perp}$ and low $v_{SP\perp}/v_{S\perp}$.

[46] The current work further shows that in nature there is a larger variety in $v_{SP\perp}$, $v_{T\perp}$ and $v_{SP\perp}/v_{S\perp}$ than observed in the models. As such, the models cannot reproduce all the complexity observed in nature, in particular asymmetric velocity distributions along individual subduction zones. However, the comparable dependence of $v_{SP\perp}$, $v_{T\perp}$ and $v_{SP\perp}/v_{S\perp}$ on D_{SE} in models and nature, as illustrated with the comparable trends of the limiting envelopes (Figure 5), does indicate a first-order control of lateral slab edges on subduction zone dynamics in nature.

[47] The models make use of a relatively weak subducting plate ($\eta_{SP}/\eta_{UM} = 1–2 \times 10^2$) and can reproduce to a large extent the range of subduction partitioning ratios observed in nature. In particular, the models reproduce high partitioning ratios ($v_{SP\perp}/v_{S\perp} \approx 1$), at which up to 100% of subduction is accommodated by trenchward subducting plate motion. In previous fully dynamic models high partitioning ratios were only reproduced with very strong plates ($\eta_{SP}/\eta_{UM} \geq 1000$), suggesting that plates in nature would have to be strong to explain the observed high partitioning ratios for some subduction zones. The current model results counter this suggestion and allow η_{SP}/η_{UM} in nature to be relatively low and of the order $1–2 \times 10^2$.

[48] **Acknowledgments.** Discussions with and feedback from Roberto Weinberg and Philippe Yamato on subduction kinematics and dynamics are greatly appreciated. Comments from two anonymous reviewers and reviewer Warren Hamilton have strengthened the paper. We would like to thank The National Computational Infrastructure and AuScope for computational resources and technical support. W.P.S. was supported by a QE II fellowship, Discovery grant DP0771823 and Discovery grant DP110103387 from the Australian Research Council, a Monash fellowship, and a J. G. Russell Award from the Australian Academy of Science.

References

Bird, P. (2003), An updated digital model of plate boundaries, *Geochem. Geophys. Geosyst.*, *4*(3), 1027, doi:10.1029/2001GC000252.

Buttles, J., and P. Olson (1998), A laboratory model of subduction zone anisotropy, *Earth Planet. Sci. Lett.*, *164*, 245–262, doi:10.1016/S0012-821X(98)00211-8.

Calmant, S., B. Pelletier, R. Pillet, M. Régnier, P. Lebellegard, D. Maillard, F. Taylor, M. Bevis, and J. Recy (1997), Interseismic and coseismic motions in GPS series related to the Ms 7.3 July 13, 1994, Malekula earthquake, central New Hebrides subduction zone, *Geophys. Res. Lett.*, *24*, 3077–3080, doi:10.1029/97GL02962.

Capitanio, F. A., G. Morra, and S. Goes (2009), Dynamics of plate bending at the trench and slab-plate coupling, *Geochem. Geophys. Geosyst.*, *10*, Q04002, doi:10.1029/2008GC002348.

Capitanio, F. A., D. R. Stegman, L. N. Moresi, and W. Sharples (2010), Upper plate controls on deep subduction, trench migrations and deformations at convergent margins, *Tectonophysics*, *483*, 80–92, doi:10.1016/j.tecto.2009.08.020.

Carlson, R. L., T. W. C. Hilde, and S. Uyeda (1983), The driving mechanism of plate tectonics: Relation to age of the lithosphere at trenches, *Geophys. Res. Lett.*, *10*, 297–300, doi:10.1029/GL010i004p00297.

Clark, S. R., D. Stegman, and R. D. Müller (2008), Episodicity in back-arc tectonic regimes, *Phys. Earth Planet. Inter.*, *171*, 265–279, doi:10.1016/j.pepi.2008.04.012.

Clift, P., and P. Vannucchi (2004), Controls on tectonic accretion versus erosion in subduction zones: Implications for the origin and recycling of the continental crust, *Rev. Geophys.*, *42*, RG2001, doi:10.1029/2003RG000127.

Cloos, M. (1993), Lithospheric buoyancy and collisional orogenesis: Subduction of oceanic plateaus, continental margins, island arcs, spreading ridges and seamounts, *Geol. Soc. Am. Bull.*, *105*, 715–737, doi:10.1130/0016-7606(1993)105<0715:LBACOS>2.3.CO;2.

Cooper, P., and B. Taylor (1987), Seismotectonics of New Guinea: A model for arc reversal following arc-continent collision, *Tectonics*, *6*, 53–67, doi:10.1029/TC006i001p00053.

Darby, D. J., and C. M. Meertens (1995), Terrestrial and GPS measurements of deformation across the Taupo back arc and Hikurangi forearc regions in New Zealand, *J. Geophys. Res.*, *100*, 8221–8232, doi:10.1029/94JB03265.

DeMets, C., R. G. Gordon, D. F. Argus, and S. Stein (1994), Effect of recent revisions to the geomagnetic reversal time scale on estimates of current plate motions, *Geophys. Res. Lett.*, *21*, 2191–2194, doi:10.1029/94GL02118.

Di Giuseppe, E., J. van Hunen, F. Funiciello, C. Faccenna, and D. Giardini (2008), Slab stiffness control of trench motion: Insights from numerical models, *Geochem. Geophys. Geosyst.*, *9*, Q02014, doi:10.1029/2007GC001776.

Dickinson, W. R., and W. S. Snyder (1979), Geometry of subducted slabs related to San Andreas transform, *J. Geol.*, *87*, 609–627, doi:10.1086/628456.

Faccenna, C., A. Heuret, F. Funiciello, S. Lallemand, and T. W. Becker (2007), Predicting trench and plate motion from the dynamics of a strong slab, *Earth Planet. Sci. Lett.*, *257*, 29–36, doi:10.1016/j.epsl.2007.02.016.

Forsyth, D. W., and S. Uyeda (1975), On the relative importance of the driving forces of plate motion, *Geophys. J. R. Astron. Soc.*, *43*, 163–200.

Funiciello, F., C. Faccenna, and D. Giardini (2004), Role of lateral mantle flow in the evolution of subduction systems: Insights from laboratory experiments, *Geophys. J. Int.*, *157*, 1393–1406, doi:10.1111/j.1365-246X.2004.02313.x.

Goes, S., F. A. Capitanio, and G. Morra (2008), Evidence of lower-mantle slab penetration phases in plate motions, *Nature*, *451*, 981–984, doi:10.1038/nature06691.

Govers, R., and M. J. R. Wortel (2005), Lithosphere tearing at STEP faults: Response to edges of subduction zones, *Earth Planet. Sci. Lett.*, *236*, 505–523, doi:10.1016/j.epsl.2005.03.022.

Gripp, A. E., and R. G. Gordon (1990), Current plate velocities relative to the hotspots incorporating the nuvel-1 global plate motion model, *Geophys. Res. Lett.*, *17*, 1109–1112, doi:10.1029/GL017i008p01109.

Gutscher, M.-A., J. Malod, J.-P. Rehault, I. Contrucci, F. Klingelhoefer, L. Mendes-Victor, and W. Spakman (2002), Evidence for active subduction beneath Gibraltar, *Geology*, *30*, 1071–1074, doi:10.1130/0091-7613(2002)030<1071:EFASBG>2.0.CO;2.

Hale, A. J., K.-D. Gottschaldt, G. Rosenbaum, L. Bourgouin, M. Bauchy, and H. Mühlhaus (2010), Dynamics of slab tear faults: Insights from numerical modelling, *Tectonophysics*, *483*, 58–70, doi:10.1016/j.tecto.2009.05.019.

Hall, R., and W. Spakman (2002), Subducted slabs beneath the eastern Indonesia-Tonga region: Insights from tomography, *Earth Planet. Sci. Lett.*, *201*, 321–336, doi:10.1016/S0012-821X(02)00705-7.

Hamilton, W. B. (2003), An alternative Earth, *GSA Today*, *13*(11), 4–12, doi:10.1130/1052-5173(2003)013<0004:AAE>2.0.CO;2.

Heuret, A., and S. Lallemand (2005), Plate motions, slab dynamics and back-arc deformation, *Phys. Earth Planet. Inter.*, *149*, 31–51, doi:10.1016/j.pepi.2004.08.022.

Jarrard, R. D. (1986), Relations among subduction parameters, *Rev. Geophys.*, *24*, 217–284, doi:10.1029/RG024i002p00217.

Kincaid, C., and R. W. Griffiths (2004), Variability in flow and temperatures within mantle subduction zones, *Geochem. Geophys. Geosyst.*, *5*, Q06002, doi:10.1029/2003GC000666.

Kozhurin, A., et al. (2006), Trenching studies of active faults in Kamchatka, eastern Russia: Paleoseismic, tectonic and hazard implications, *Tectonophysics*, *417*, 285–304, doi:10.1016/j.tecto.2006.01.004.

Kreemer, C., W. E. Holt, and A. J. Haines (2003), An integrated global model of present-day plate motions and plate boundary deformation, *Geophys. J. Int.*, *154*, 8–34, doi:10.1046/j.1365-246X.2003.01917.x.

Lawver, L. A., R. A. Keller, M. R. Fisk, and J. A. Strelin (1995), Bransfield Strait, Antarctic Peninsula, active extension behind a dead arc, in *Backarc Basins: Tectonics and Magmatism*, edited by B. Taylor, pp. 315–342, Plenum, New York, doi:10.1007/978-1-4615-1843-3_8.

Lebrun, J.-F., G. Lamarche, J.-Y. Collot, and J. Delteil (2000), Abrupt strike-slip fault to subduction transition: The Alpine fault-Puysegur trench connection, New Zealand, *Tectonics*, *19*, 688–706, doi:10.1029/2000TC900008.

Loiselet, C., L. Husson, and J. Braun (2009), From longitudinal slab curvature to slab rheology, *Geology*, *37*, 747–750, doi:10.1130/G30052A.1.

Long, M. D., and P. G. Silver (2008), The subduction zone flow field from seismic anisotropy: A global view, *Science*, *319*, 315–318, doi:10.1126/science.1150809.

Magee, M. E., and M. D. Zoback (1993), Evidence for a weak interplate thrust fault along the northern Japan subduction zone and implications for the mechanics of thrust faulting and fluid expulsion, *Geology*, *21*, 809–812, doi:10.1130/0091-7613(1993)021<0809:EFAWIT>2.3.CO;2.

Mason, W. G., L. Moresi, P. G. Betts, and M. S. Miller (2010), Three-dimensional numerical models of the influence of a buoyant oceanic plateau on subduction zones, *Tectonophysics*, *483*, 71–79, doi:10.1016/j.tecto.2009.08.021.

Mazzotti, S., P. Henry, and X. Le Pichon (2001), Transient and permanent deformation of central Japan estimated by GPS 2. Strain partitioning and arc-arc collision, *Earth Planet. Sci. Lett.*, *184*, 455–469, doi:10.1016/S0012-821X(00)00336-8.

McClusky, S., et al. (2000), Global positioning system constraints on plate kinematics and dynamics in the eastern Mediterranean and Caucasus, *J. Geophys. Res.*, *105*, 5695–5719.

Millen, D. W., and M. W. Hamburger (1998), Seismological evidence for tearing of the Pacific plate at the northern termination of the Tonga subduction zone, *Geology*, *26*, 659–662, doi:10.1130/0091-7613(1998)026<0659:SEFTOT>2.3.CO;2.

Molnar, P., and T. Atwater (1978), Interarc spreading and Cordilleran tectonics as alternates related to the age of subducted oceanic lithosphere, *Earth Planet. Sci. Lett.*, *41*, 330–340, doi:10.1016/0012-821X(78)90187-5.

Moresi, L., and V. Solomatov (1998), Mantle convection with a brittle lithosphere: Thoughts on the global tectonic styles of the Earth and Venus, *Geophys. J. Int.*, *133*, 669–682, doi:10.1046/j.1365-246X.1998.00521.x.

Moresi, L., F. Dufour, and H.-B. Mühlhaus (2003), A Lagrangian integration point finite element method for large deformation modeling of viscoelastic geomaterials, *J. Comput. Phys.*, *184*, 476–497, doi:10.1016/S0021-9991(02)00031-1.

Morra, G., K. Regenauer-Lieb, and D. Giardini (2006), Curvature of oceanic arcs, *Geology*, *34*, 877–880, doi:10.1130/G22462.1.

Morra, G., L. Quevedo, N. Butterworth, K. J. Matthews, and D. Müller (2010), Global dynamic numerical simulations of plate tectonic reorganizations, Abstract U51A–0008 presented at 2010 Fall Meeting, AGU, San Francisco, Calif., 13–17 Dec.

Nilforoushan, F., et al. (2003), GPS network monitors the Arabia-Eurasia collision deformation in Iran, *J. Geod.*, *77*, 411–422, doi:10.1007/s00190-003-0326-5.

Nishimura, S., M. Hashimoto, and M. Ando (2004), A rigid block rotation model for the GPS derived velocity field along the Ryukyu arc, *Phys. Earth Planet. Inter.*, *142*, 185–203, doi:10.1016/j.pepi.2003.12.014.

Norabuena, E., L. Leffler-Griffin, A. Mao, T. Dixon, S. Stein, I. Selwyn Sacks, L. Ocola, and M. Ellis (1998), Space geodetic observations of Nazca-South America convergence across the central Andes, *Science*, *279*, 358–362, doi:10.1126/science.279.5349.358.

O'Neill, C., D. Müller, and B. Steinberger (2005), On the uncertainties in hot spot reconstructions and the significance of moving hot spot reference frames, *Geochem. Geophys. Geosyst.*, *6*, Q04003, doi:10.1029/2004GC000784.

OzBench, M., et al. (2008), A model comparison study of large-scale mantle–lithosphere dynamics driven by subduction, *Phys. Earth Planet. Inter.*, *171*, 224–234, doi:10.1016/j.pepi.2008.08.011.

Rangin, C., X. Le Pichon, S. Mazzotti, M. Pubellier, N. Chamot-Rooke, M. Aurelio, A. Walpersdorf, and R. Quebral (1999), Plate convergence measured by GPS across the Sundaland/Philippine Sea Plate deformed boundary: The Philippines and eastern Indonesia, *Geophys. J. Int.*, *139*, 296–316, doi:10.1046/j.1365-246x.1999.00969.x.

Ribe, N. M. (2010), Bending mechanics and mode selection in free subduction: A thin-sheet analysis, *Geophys. J. Int.*, *180*, 559–576, doi:10.1111/j.1365-246X.2009.04460.x.

Rosenbaum, G., and G. S. Lister (2004), Neogene and Quaternary rollback evolution of the Tyrrhenian Sea, the Apennines, and the Sicilian Maghrebides, *Tectonics*, *23*, TC1013, doi:10.1029/2003TC001518.

Rosenbaum, G., M. Gasparon, F. P. Lucente, A. Peccerillo, and M. S. Miller (2008), Kinematics of slab tear faults during subduction segmentation and implications for Italian magmatism, *Tectonics*, *27*, TC2008, doi:10.1029/2007TC002143.

Russo, R. M., and P. G. Silver (1994), Trench-parallel flow beneath the Nazca Plate from seismic anisotropy, *Science*, *263*, 1105–1111, doi:10.1126/science.263.5150.1105.

Schellart, W. P. (2004), Kinematics of subduction and subduction-induced flow in the upper mantle, *J. Geophys. Res.*, *109*, B07401, doi:10.1029/2004JB002970.

Schellart, W. P. (2008a), Kinematics and flow patterns in deep mantle and upper mantle subduction models: Influence of the mantle depth and slab to mantle viscosity ratio, *Geochem. Geophys. Geosyst.*, *9*, Q03014, doi:10.1029/2007GC001656.

Schellart, W. P. (2008b), Subduction zone trench migration: Slab driven or overriding-plate-driven?, *Phys. Earth Planet. Inter.*, *170*, 73–88, doi:10.1016/j.pepi.2008.07.040.

Schellart, W. P. (2008c), Overriding plate shortening and extension above subduction zones: A parametric study to explain formation of the Andes mountains, *Geol. Soc. Am. Bull.*, *120*, 1441–1454, doi:10.1130/B26360.1.

Schellart, W. P. (2010), Evolution of subduction zone curvature and its dependence on the trench velocity and the slab to upper mantle viscosity ratio, *J. Geophys. Res.*, *115*, B11406, doi:10.1029/2009JB006643.

Schellart, W. P. (2011), A subduction zone reference frame based on slab geometry and subduction partitioning of plate motion and trench migration, *Geophys. Res. Lett.*, *38*, L16317, doi:10.1029/2011GL048197.

Schellart, W. P., J. Freeman, D. R. Stegman, L. Moresi, and D. May (2007), Evolution and diversity of subduction zones controlled by slab width, *Nature*, *446*, 308–311, doi:10.1038/nature05615.

Schellart, W. P., D. R. Stegman, and J. Freeman (2008), Global trench migration velocities and slab migration induced upper mantle volume fluxes: Constraints to find an Earth reference frame based on minimizing viscous dissipation, *Earth Sci. Rev.*, *88*, 118–144, doi:10.1016/j.earscirev.2008.01.005.

Schellart, W. P., D. R. Stegman, R. J. Farrington, J. Freeman, and L. Moresi (2010), Cenozoic tectonics of western North America controlled by evolving width of Farallon slab, *Science*, *329*, 316–319, doi:10.1126/science.1190366.

Seno, T., S. Stein, and A. E. Gripp (1993), A model for the motion of the Philippine Sea plate consistent with NUVEL-1 and geological data, *J. Geophys. Res.*, *98*, 17,941–17,948, doi:10.1029/93JB00782.

Stegman, D. R., M. A. Richards, and J. R. Baumgardner (2002), Effects of depth-dependent viscosity and plate motions on maintaining a relatively uniform mid-ocean ridge basalt reservoir in whole mantle flow, *J. Geophys. Res.*, *107*(B6), 2116, doi:10.1029/2001JB000192.

Stegman, D. R., J. Freeman, W. P. Schellart, L. Moresi, and D. May (2006), Influence of trench width on subduction hinge retreat rates in 3-D models of slab rollback, *Geochem. Geophys. Geosyst.*, *7*, Q03012, doi:10.1029/2005GC001056.

Stegman, D. R., R. Farrington, F. A. Capitanio, and W. P. Schellart (2010a), A regime diagram for subduction styles from 3-D numerical models of free subduction, *Tectonophysics*, *483*, 29–45, doi:10.1016/j.tecto.2009.08.041.

Stegman, D. R., W. P. Schellart, and J. Freeman (2010b), Competing influences of plate width and far-field boundary conditions on trench migration and morphology of subducted slabs in the upper mantle, *Tectonophysics*, *483*, 46–57, doi:10.1016/j.tecto.2009.08.026.

Suter, M., M. L. Martínez, O. Q. Legorreta, and M. C. Martínez (2001), Quaternary intra-arc extension in the central Trans-Mexican volcanic belt, *Geol. Soc. Am. Bull.*, *113*, 693–703, doi:10.1130/0016-7606(2001)113<0693:QIAEIT>2.0.CO;2.

Taylor, F. W., et al. (1995), Geodetic measurements of convergence at the New Hebrides island arc indicate arc fragmentation caused by an impinging aseismic ridge, *Geology*, *23*, 1011–1014, doi:10.1130/0091-7613(1995)023<1011:GMOCAT>2.3.CO;2.

Thomas, C., R. Livermore, and F. Pollitz (2003), Motion of the Scotia Sea plates, *Geophys. J. Int.*, *155*, 789–804, doi:10.1111/j.1365-246X.2003.02069.x.

Thorkelson, D. J. (1996), Subduction of diverging plates and the principles of slab window formation, *Tectonophysics*, *255*, 47–63, doi:10.1016/0040-1951(95)00106-9.

Thorkelson, D. J., J. K. Madsen, and C. L. Sluggett (2011), Mantle flow through the northern cordilleran slab window revealed by volcanic geochemistry, *Geology*, *39*, 267–270, doi:10.1130/G31522.1.

Tregoning, P., et al. (1998), Estimation of current plate motions in Papua New Guinea from Global Positioning System observations, *J. Geophys. Res.*, *103*, 12,181–12,203, doi:10.1029/97JB03676.

Tregoning, P., R. J. Jackson, H. McQueen, K. Lambeck, C. Stevens, R. P. Little, R. Curley, and R. Rosa (1999), Motion of the South Bismarck plate, Papua New Guinea, *Geophys. Res. Lett.*, *26*, 3517–3520, doi:10.1029/1999GL010840.

van der Hilst, R., and P. Mann (1994), Tectonic implications of tomographic images of subducted lithosphere beneath northwestern South America, *Geology*, *22*, 451–454, doi:10.1130/0091-7613(1994)022<0451:TIOTIO>2.3.CO;2.

van Dinther, Y., G. Morra, F. Funiciello, and C. Faccenna (2010), Role of the overriding plate in the subduction process: Insights from numerical models, *Tectonophysics*, *484*, 74–86, doi:10.1016/j.tecto.2009.08.038.

van Keken, P. E., E. H. Hauri, and C. J. Ballentine (2002), Mantle mixing: The generation, preservation, and destruction of chemical heterogeneity, *Annu. Rev. Earth Planet. Sci.*, *30*, 493–525, doi:10.1146/annurev.earth.30.091201.141236.

Wang, K., T. Mulder, G. C. Rogers, and R. D. Hyndman (1995), Case for very low coupling stress on the Cascadia subduction fault, *J. Geophys. Res.*, *100*, 12,907–12,918, doi:10.1029/95JB00516.

Wells, R., C. S. Weaver, and R. J. Blakely (1998), Fore-arc migration in Cascadia and its neotectonic significance, *Geology*, *26*, 759–762, doi:10.1130/0091-7613(1998)026<0759:FAMICA>2.3.CO;2.

Wessel, P., Y. Harada, and L. W. Kroenke (2006), Toward a self-consistent, high-resolution absolute plate motion model for the Pacific, *Geochem. Geophys. Geosyst.*, *7*, Q03L12, doi:10.1029/2005GC001000.

Wortel, R., R. Govers, and W. Spakman (2009), Continental collision and the STEP-wise evolution of convergent plate boundaries: From structure to dynamics, in *Subduction Zone Geodynamics*, edited by S. Lallemand and F. Funiciello, pp. 47–59, Springer, Berlin, doi:10.1007/978-3-540-87974-9.

Wright, I. C. (1993), Pre-spread rifting and heterogeneous volcanism in the southern Havre Trough back-arc basin, *Mar. Geol.*, *113*, 179–200, doi:10.1016/0025-3227(93)90017-P.

Wu, B., C. P. Conrad, A. Heuret, C. Lithgow-Bertelloni, and S. Lallemand (2008), Reconciling strong slab pull and weak plate bending: The plate motion constraint on the strength of mantle slabs, *Earth Planet. Sci. Lett.*, *272*, 412–421, doi:10.1016/j.epsl.2008.05.009.

Yamato, P., L. Husson, J. Braun, C. Loiselet, and C. Thieulot (2009), Influence of surrounding plates on 3D subduction dynamics, *Geophys. Res. Lett.*, *36*, L07303, doi:10.1029/2008GL036942.

Yang, T., S. P. Grand, D. Wilson, M. Guzman-Speziale, J. M. Gomez-Gonzalez, T. Dominguez-Reyes, and J. Ni (2009), Seismic structure beneath the Rivera subduction zone from finite-frequency seismic tomography, *J. Geophys. Res.*, *114*, B01302, doi:10.1029/2008JB005830.

Zellmer, K. E., and B. Taylor (2001), A three-plate kinematic model for Lau Basin opening, *Geochem. Geophys. Geosyst.*, *2*, 1020, doi:10.1029/2000GC000106.

Zhong, S., and M. Gurnis (1995), Mantle convection with plates and mobile, faulted plate margins, *Science*, *267*, 838–843, doi:10.1126/science.267.5199.838.

R. J. Farrington, School of Mathematical Sciences, Monash University, Melbourne, VIC 3800, Australia.

L. Moresi and W. P. Schellart, School of Geosciences, Monash University, Melbourne, VIC 3800, Australia. (wouter.schellart@monash.edu)

D. R. Stegman, Scripps Institution of Oceanography, University of California, San Diego, La Jolla, CA 92093, USA.